

# Structure-Guided Histopathology Synthesis via Dual-LoRA Diffusion

Xuan Xu and Prateek Prasanna

Stony Brook University

xuanxu@cs.stonybrook.edu, prateek.prasanna@stonybrook.edu

**Abstract.** Histopathology image synthesis plays an important role in tissue restoration, data augmentation, and modeling of tumor microenvironments. However, existing generative methods typically address restoration and generation as separate tasks, although both share the same objective of structure-consistent tissue synthesis under varying degrees of missingness, and often rely on weak or inconsistent structural priors that limit realistic cellular organization.

We propose **Dual-LoRA Controllable Diffusion**, a unified centroid-guided diffusion framework that jointly supports *Local Structure Completion* and *Global Structure Synthesis* within a single model. Multi-class nuclei centroids serve as lightweight and annotation-efficient spatial priors, providing biologically meaningful guidance under both partial and complete image absence. Two task-specific LoRA adapters specialize the shared backbone for local and global objectives without retraining separate diffusion models. Extensive experiments demonstrate consistent improvements over state-of-the-art GAN and diffusion baselines across restoration and synthesis tasks. For local completion, LPIPS computed within the masked region improves from 0.1797 (HARP) to 0.1524, and for global synthesis, FID improves from 225.15 (CoSys) to 76.04, indicating improved structural fidelity and realism. Our approach achieves more faithful structural recovery in masked regions and substantially improved realism and morphology consistency in full synthesis, supporting scalable pan-cancer histopathology modeling.

**Keywords:** Histopathology · Diffusion models · Image synthesis.

## 1 Introduction

Whole-slide imaging (WSI) enables high-resolution visualization of tissue specimens and has become a cornerstone of modern cancer diagnosis and computational pathology [9,3,13]. However, real-world WSIs exhibit substantial variability in staining protocols, tissue architecture, and cell density across organs and cancer types. They are further affected by artifacts such as stain inconsistency, blur, folds, foreign objects, and missing regions [17,19]. These degradations often occur in diagnostically critical areas and complicate both expert interpretation and downstream computational analysis.

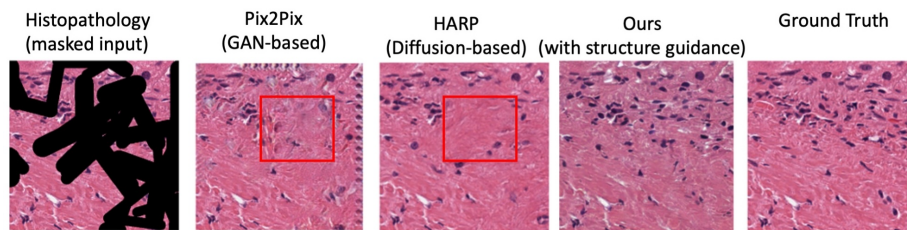


**Fig. 1.** Challenges in histopathology local structure completion with complex masks. Pix2Pix [8] and HARP [4] fail to reconstruct fine-grained structures under large irregular masks, while our method preserves coherent morphology and tissue continuity. Red boxes highlight reconstruction failures in the baselines.

Generative models have emerged as a promising solution for histopathology image restoration and data augmentation [10,23,11]. Existing approaches address tasks such as artifact removal, stain normalization, cell layout generation, or patch-level synthesis [4,16,22,21]. Despite encouraging results, most methods rely primarily on pixel-level inputs or global embeddings, lacking explicit spatial guidance of cellular organization [25,4]. As a result, when reconstructing large missing regions or synthesizing tissue from limited cues, they may generate morphologically implausible structures ( Fig. 1). In practice, histopathology synthesis tasks typically arise in two closely related scenarios depending on the extent of missing tissue: **(1) Local Structure Completion**, where partially missing tissue regions are reconstructed while preserving the surrounding histomorphology, and **(2) Global Structure Synthesis**, where an entire tissue patch is generated solely from structural priors when image content is fully absent. Although typically treated as separate problems, both share a common objective: generating morphologically realistic H&E tissue consistent with a biologically meaningful structural prior.

We argue that explicit spatial priors are essential for realistic synthesis in computational pathology. Dense annotations such as nuclei segmentation masks provide detailed structural information but are costly to obtain at scale [1]. Self-supervised embeddings capture global context yet lack fine-grained cellular layout cues [25]. In contrast, *cell-type centroids* offer a lightweight and annotation-efficient representation of nuclei location, density, and coarse cell identity. They encode biologically meaningful spatial organization while remaining scalable across pan-cancer datasets. Diffusion models naturally support flexible conditional generation and spatial control, making them well-suited for integrating such structured priors in histopathology synthesis [15,26].

Building upon this observation, we present **Dual-LoRA Controllable Diffusion**, a unified centroid-guided diffusion framework that supports both local structure completion and global structure synthesis within a single model. A shared morphology-aware backbone provides consistent structural reasoning across cancer types, while two lightweight LoRA adapters [7,24] specialize the

model for the distinct optimization characteristics of the two tasks. This design enables task-specific adaptation without training separate diffusion models, promoting parameter efficiency and cross-task knowledge sharing.

We train and evaluate our framework on a large-scale pan-cancer dataset spanning 30+ cancer types [20], covering diverse organs, stain variations, and tissue architectures. Unlike prior work that typically focuses on a single cancer type or low-resolution patches (such as  $128 \times 128$  or  $256 \times 256$ ) [4,12], our model operates at a resolution of  $512 \times 512$  and jointly supports both local structure completion and global structure synthesis within a unified framework. Across both tasks, Dual-LoRA Controllable Diffusion consistently outperforms state-of-the-art GAN- and diffusion-based baselines under generic image quality metrics as well as pathology-aware evaluations. Downstream classification experiments further demonstrate improved preservation of discriminative histomorphology across cancer types.

Our contributions are summarized as follows:

- **Centroid-guided unified diffusion backbone.** We propose a structure-aware generative framework that jointly supports local structure completion and global structure synthesis across 30+ cancer types using multi-class nuclei centroids as scalable spatial priors.
- **Dual-LoRA specialization within a unified framework.** Two lightweight LoRA adapters enable task-specific optimization for local structure completion and global structure synthesis while sharing a common morphology-aware backbone.
- **Comprehensive evaluation across restoration and synthesis tasks.** Extensive experiments demonstrate consistent improvements over strong GAN and diffusion baselines on both inpainting and full synthesis tasks under generic and pathology-aware metrics.

## 2 Methods

Our proposed **Dual-LoRA Controllable Diffusion**, a centroid-guided latent diffusion framework, unifies two synthesis modes: (i) *Local Structure Completion* and (ii) *Global Structure Synthesis*. Both modes share a frozen Stable Diffusion backbone with ControlNet-based spatial conditioning [26], while two lightweight LoRA adapters enable task-specific specialization within a single architecture ( Fig. 2).

### 2.1 Unified Problem Formulation

Let  $x \in \mathbb{R}^{H \times W \times 3}$  denote an H&E image of spatial resolution  $H \times W$ ,  $C \in \mathbb{R}^{H \times W \times K}$  denote  $K$  cell-type centroid maps,  $m \in \{0, 1\}^{H \times W}$  a binary mask indicating missing regions, and  $p$  a text prompt encoding high-level tissue semantics.

We unify both tasks through a single spatial control tensor:

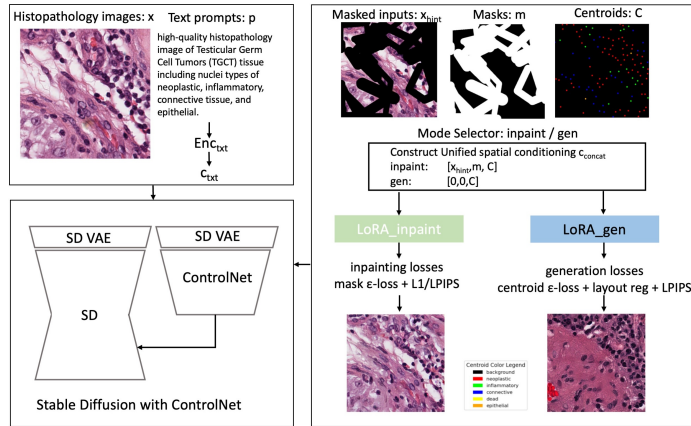


**Fig. 2.** Overview of Dual-LoRA Controllable Diffusion. Given image  $x$ , mask  $m$ , and centroid maps  $C$ , we build a unified spatial condition. For inpainting,  $[x_{hint}, m, C]$  with  $x_{hint} = x \odot (1 - m)$ ; for generation,  $[0, 0, C]$ . Stable Diffusion and ControlNet are frozen, while two LoRA adapters specialize the two modes.

$$c_{concat}^{(s)} = [x_{hint}^{(s)}, m^{(s)}, C], \quad s \in \{\text{inpaint}, \text{gen}\}.$$

For inpainting,

$$x_{hint}^{(\text{inpaint})} = x \odot (1 - m), \quad m^{(\text{inpaint})} = m.$$

For generation,

$$x_{hint}^{(\text{gen})} = \mathbf{0}, \quad m^{(\text{gen})} = \mathbf{0}.$$

Thus, both modes share identical structural priors  $C$ , differing only in whether visual evidence is provided.

We follow latent diffusion [15], where  $z_t$  is denoised as

$$\epsilon_\theta = \epsilon_\theta(z_t, t; c_{concat}^{(s)}, c_{txt}; \phi^{(s)}).$$

The text embedding  $c_{txt} = Enc_{c_{txt}}(p)$  is obtained using the frozen CLIP encoder from Stable Diffusion v1.5 [14,15], where  $p$  encodes cancer-type and centroid semantics.

## 2.2 Dual-LoRA Specialization

Local completion emphasizes high-resolution texture recovery, whereas global synthesis requires large-scale spatial organization from centroids alone. Training a single parameterization for both leads to competing gradients.

Inspired by CtrLoRA [24], we attach two lightweight LoRA adapters [7] to the linear layers of the ControlNet [26], denoted as  $\phi^{(\text{inpaint})}$  and  $\phi^{(\text{gen})}$ . For

each backbone weight  $W$ , the effective weight becomes  $W_{\text{eff}}^{(s)} = W + B^{(s)}A^{(s)}$ , where only  $A^{(s)}$  and  $B^{(s)}$  are trainable. During training, only the active adapter receives gradient updates, preserving a shared morphology-aware representation while enabling task-specific modulation.

### 2.3 Local Structure Completion

The inpainting branch reconstructs masked tissue regions using both visible context and centroid priors. Centroids provide structural guidance inside the hole region, while visible tissue ensures boundary consistency.

*Mask-aware diffusion loss.* We emphasize masked regions during denoising by applying a spatially weighted  $\epsilon$ -prediction loss:

$$\mathcal{L}_{\text{eps}}^{\text{inpaint}} = \|(\epsilon - \hat{\epsilon}) \odot w_{\text{mask}} \odot w_{\text{snr}}\|_2^2,$$

where  $w_{\text{mask}}$  increases gradients inside missing regions and  $w_{\text{snr}}$  follows the Min-SNR reweighting strategy [6].

*Image-domain refinement.* To improve perceptual fidelity within the hole, we decode the clean prediction  $\hat{x}_0$  from latent space and introduce a softened mask  $m_{\text{soft}}$  to restrict image-level supervision to the missing region:

$$\mathcal{L}_{\text{img}} = \lambda_{L1} \|(\hat{x}_0 - x) \odot m_{\text{soft}}\|_1 + \lambda_{\text{LPIPS}} \text{LPIPS}(\hat{x}_0, x).$$

The perceptual term[27] is activated after a warm-up phase to avoid destabilizing early diffusion training.

*Final objective.*

$$\mathcal{L}_{\text{inpaint}} = \mathcal{L}_{\text{eps}}^{\text{inpaint}} + \mathcal{L}_{\text{img}}.$$

By combining masked observations with centroid-based structural priors, the model learns to reconstruct missing tissue while preserving cellular organization. The centroids reduce structural hallucination under large occlusions and promote anatomically consistent completions.

### 2.4 Global Structure Synthesis

The generation branch synthesizes complete histopathology images from centroid priors and text semantics, without any observed pixels. Unlike inpainting, all structural information must be inferred from  $C$ , requiring explicit spatial guidance to ensure biologically plausible organization.

*Centroid-aware diffusion loss.* We adopt an  $\epsilon$ -prediction loss with spatial weighting to emphasize structurally meaningful regions:

$$\mathcal{L}_{\text{eps}}^{\text{gen}} = \|(\epsilon - \hat{\epsilon}) \odot w_{\text{snr}} \odot w_{\text{cent}}\|_2^2,$$

where  $w_{\text{snr}}$  follows Min-SNR reweighting [6], and  $w_{\text{cent}}$  assigns higher weights near centroid locations, encouraging coherent cellular organization during denoising.

*Layout regularization.* To further stabilize global structure, we attach a lightweight layout head that predicts centroid-activation maps  $\hat{C} \in [0, 1]^{K \times H \times W}$  from ControlNet features. We impose an inter-class separation penalty [21]:

$$\mathcal{L}_{\text{inter}} = \frac{2}{K(K-1)} \sum_{i < j} \frac{\langle \hat{C}_i, \hat{C}_j \rangle}{HW},$$

which discourages spatial overlap across cell types and promotes structurally consistent layouts.

*Final objective.* The overall generation loss combines diffusion supervision and structural regularization:

$$\mathcal{L}_{\text{gen}} = \mathcal{L}_{\text{eps}}^{\text{gen}} + w_{\text{inter}} \mathcal{L}_{\text{inter}} + \lambda_{\text{LPIPS}} \text{LPIPS}.$$

A very weak perceptual term is applied only after warm-up to suppress minor visual artifacts without overriding structural guidance.

### 3 Experiments and Results

#### 3.1 Dataset

We construct a large-scale pan-cancer histopathology dataset from TCGA [20], including 214,030 training patches from 7,245 whole-slide images (WSIs) spanning 31 cancer types, and 2,343 test patches from 18 WSIs covering 7 representative cancer types. All patches are  $512 \times 512$  at  $40\times$  magnification. Nuclei are segmented using HoVer-Net [5].

For each nucleus we extract its class among five categories and its centroid, which are rasterized into  $K = 5$  centroid maps used as structural priors. Text prompts encode cancer type and nuclei-class semantics.

#### 3.2 Implementation Details

We build upon Stable Diffusion v1.5 [15] with a frozen ControlNet backbone [24]. Two rank-256 LoRA adapters are trained while the backbone remains fixed, yielding  $\sim 113\text{M}$  trainable parameters ( $< 10\%$  of full model). Training runs for 150k steps on three RTX 8000 GPUs with alternating modes.

Method	Condition	FID(full) $\downarrow$	IS(full) $\uparrow$	LPIPS-FSD(full) $\downarrow$	LPIPS(mask) $\downarrow$	UNI-LPIPS(mask) $\downarrow$	SSIM(mask) $\uparrow$	PSNR(mask) $\uparrow$
Pix2Pix (GAN-based) [8]	Masked input	66.21	2.23	0.7847	0.1538	0.4827	<b>0.5316</b> *	<b>17.53</b> *
HARP (Diffusion-based) [4]	Masked input	60.27	2.19	0.4967*	0.1797	0.4664	<b>0.5247</b>	<b>16.29</b>
Ours (Inpaint)	Prompt+Masked input	<b>49.10</b>	<b>3.51</b> *	0.6296	<b>0.1524</b>	<b>0.4414</b>	0.4923	15.38
Ours (Inpaint)	Prompt+ Masked input + Centroids	<b>37.39</b> *	<b>3.08</b>	<b>0.4800</b> *	<b>0.1432</b> *	<b>0.4321</b> *	0.5014	15.90

**Table 1.** Quantitative comparison for local structure completion.

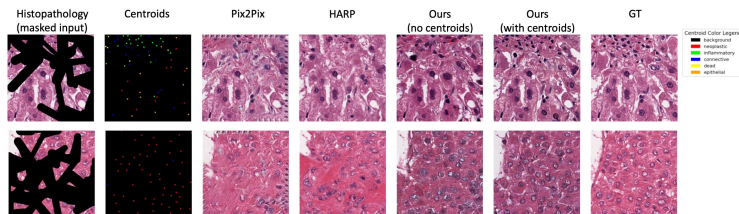


Fig. 3. Qualitative comparison on inpainting under centroid-guided control.

Method	Condition	FID↓	IS↑	LPIPS-FSD↓	UNI-FSD↓	UNI-LPIPS↓
Pix2Pix (GAN-based) [8]	Centroids	98.45	1.76	2.20	331.15	0.9159
CoSys (Diffusion-based) [12]	Prompt + Centroids	225.15	2.27	5.04	331.58	0.9448
Ours (Gen)	Prompt + Centroids	<b>76.04</b>	<b>3.26</b>	<b>2.04</b>	<b>291.85</b>	<b>0.9055</b>

Table 2. Quantitative comparison of centroid-guided global structure synthesis.

### 3.3 Local Structure Completion

*Quantitative results.* Table 1 reports both full-image and mask-region metrics. In realistic settings where centroid annotations are unavailable at inference time, our model—trained with centroid-informed priors—already outperforms representative GAN-based methods such as Pix2Pix [8] and the state-of-the-art diffusion-based approach HARP [4] in FID and LPIPS-based metrics. With centroid guidance, performance further improves, achieving the best FID (37.39), LPIPS (mask) (0.1432), and UNI-LPIPS (mask) (0.4321).

Perceptual metrics consistently favor our method, while SSIM and PSNR are reported for completeness but correlate weakly with diagnostic realism [23].

*Qualitative results.* As shown in Fig. 3, Pix2Pix [8] exhibits banding artifacts and HARP [4] produces oversmoothed textures. Our model restores realistic stain variation and sharp nuclear boundaries, with centroid guidance improving structural coherence.

### 3.4 Global Structure Synthesis

*Quantitative results.* Table 2 summarizes centroid-guided full-image synthesis. Our method achieves the best performance across all generic and pathology-aware metrics. Compared to the recent diffusion-based baseline CoSys [12], FID

Method	Condition	Accuracy↑	Balanced Acc↑	Kappa↑	Weighted F1↑
Pix2Pix (GAN-based) [8]	Centroids	0.5168	0.4717	-0.0542	0.5249
CoSys (Diffusion-based) [12]	Prompt + Centroids	0.8909	0.8822	0.7552	0.8915
Ours (Gen)	Prompt + Centroids	<b>0.9506</b>	<b>0.9612</b>	<b>0.8916</b>	<b>0.9513</b>

Table 3. Downstream cancer-type classification on synthetic LIHC and MESO patches. Our model outperforms Pix2Pix [8] and CoSys [12] across all metrics.

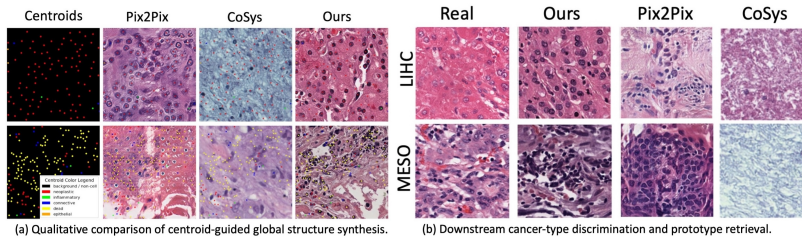


**Fig. 4.** Qualitative evaluation of centroid-guided global structure synthesis. (a) Under centroid guidance, Dual-LoRA produces coherent H&E morphology compared to Pix2Pix and CoSys. (b) Downstream cancer-type discrimination (LIHC, MESO) shows preservation of class-specific morphology.

improves from 225.15 to 76.04 and LPIPS-FSD from 5.04 to 2.04, indicating substantial gains in realism and structural consistency. UNI-FSD and UNI-LPIPS computed using the UNI-2h encoder [2] further confirm improved histomorphology preservation.

*Qualitative results.* Fig. 4 (a) shows that Pix2Pix [8] introduces artifacts and ignores layout, while CoSys [12] often collapses into blurred regions. Our model produces coherent cellular organization aligned with centroid guidance.

**Downstream Cancer-Type Classification.** To assess whether synthetic images preserve discriminative morphology, we classify LIHC and MESO patches using UNI-2h embeddings [2] and ProtoNet [18] in a proof-of-concept study. As shown in Table 3, Dual-LoRA achieves the highest balanced accuracy (0.96) and weighted F1 (0.95), improving over CoSys by approximately 9% in balanced accuracy and 6.7% in weighted F1. These results demonstrate that our framework best preserves cancer-type-specific histomorphology.

## 4 Conclusion

We presented **Dual-LoRA Controllable Diffusion**, a unified framework for structure-guided histopathology synthesis across pan-cancer data. By integrating centroid-based priors with a shared diffusion backbone and two lightweight LoRA adapters, the model supports both local completion and global synthesis within a single architecture. Experiments demonstrate improved realism and morphological fidelity over strong GAN and diffusion baselines. Centroid priors can be obtained from automated segmentation or layout-generation models such as TopoCellGen [21], enabling scalable and controllable histopathology simulation. This flexibility makes the proposed framework scalable for data augmentation, simulation, and educational applications in computational pathology.

## References

1. Abdelsamea, M.M., Zidan, U., Senousy, Z., Gaber, M.M., Rakha, E., Ilyas, M.: A survey on artificial intelligence in histopathology image analysis. *Wiley Interdisciplinary Reviews: Data Mining and Knowledge Discovery* **12**(6), e1474 (2022)
2. Chen, R.J., Ding, T., Lu, M.Y., Williamson, D.F., Jaume, G., Chen, B., Zhang, A., Shao, D., Song, A.H., Shaban, M., et al.: Towards a general-purpose foundation model for computational pathology. *Nature Medicine* (2024)
3. Cheng, J., Han, Z., Mehra, R., Shao, W., Cheng, M., Feng, Q., Ni, D., Huang, K., Cheng, L., Zhang, J.: Computational analysis of pathological images enables a better diagnosis of tfe3 xp11. 2 translocation renal cell carcinoma. *Nature communications* **11**(1), 1778 (2020)
4. Fuchs, M., Sivakumar, S.K.R., Schöber, M., Woltering, N., Eich, M.L., Schweizer, L., Mukhopadhyay, A.: Harp: Unsupervised histopathology artifact restoration. In: *Medical Imaging with Deep Learning*. pp. 465–479. PMLR (2024)
5. Graham, S., Vu, Q.D., Raza, S.E.A., Azam, A., Tsang, Y.W., Kwak, J.T., Rajpoot, N.: Hover-net: Simultaneous segmentation and classification of nuclei in multi-tissue histology images. *Medical image analysis* **58**, 101563 (2019)
6. Hang, T., Gu, S., Li, C., Bao, J., Chen, D., Hu, H., Geng, X., Guo, B.: Efficient diffusion training via min-snr weighting strategy. In: *Proceedings of the IEEE/CVF international conference on computer vision*. pp. 7441–7451 (2023)
7. Hu, E.J., Shen, Y., Wallis, P., Allen-Zhu, Z., Li, Y., Wang, S., Wang, L., Chen, W.: Lora: Low-rank adaptation of large language models. *arXiv preprint arXiv:2106.09685* (2021)
8. Isola, P., Zhu, J.Y., Zhou, T., Efros, A.A.: Image-to-image translation with conditional adversarial networks. In: *Proceedings of the IEEE conference on computer vision and pattern recognition*. pp. 1125–1134 (2017)
9. Janowczyk, A., Madabhushi, A.: Deep learning for digital pathology image analysis: A comprehensive tutorial with selected use cases. *Journal of pathology informatics* **7**(1), 29 (2016)
10. Jose, L., Liu, S., Russo, C., Nadort, A., Di Ieva, A.: Generative adversarial networks in digital pathology and histopathological image processing: a review. *Journal of Pathology Informatics* **12**(1), 43 (2021)
11. Li, W., Li, J., Polson, J., Wang, Z., Speier, W., Arnold, C.: High resolution histopathology image generation and segmentation through adversarial training. *Medical Image Analysis* **75**, 102251 (2022)
12. Min, S., Oh, H.J., Jeong, W.K.: Co-synthesis of histopathology nuclei image-label pairs using a context-conditioned joint diffusion model. In: *European Conference on Computer Vision*. pp. 146–162. Springer (2024)
13. Pantanowitz, L., Valenstein, P.N., Evans, A.J., Kaplan, K.J., Pfeifer, J.D., Wilbur, D.C., Collins, L.C., Colgan, T.J.: Review of the current state of whole slide imaging in pathology. *Journal of pathology informatics* **2**(1), 36 (2011)
14. Radford, A., Kim, J.W., Hallacy, C., Ramesh, A., Goh, G., Agarwal, S., Sastry, G., Askell, A., Mishkin, P., et al.: Learning transferable visual models from natural language supervision. In: *ICML* (2021)
15. Rombach, R., Blattmann, A., Lorenz, D., Esser, P., Ommer, B.: High-resolution image synthesis with latent diffusion models (2021)
16. Rong, R., Wang, S., Zhang, X., Wen, Z., Cheng, X., Jia, L., Yang, D.M., Xie, Y., Zhan, X., Xiao, G.: Enhanced pathology image quality with restore-generative adversarial network. *The American Journal of Pathology* **193**(4), 404–416 (2023)

17. Seoane, J., Varela-Centelles, P., Ramírez, J., Cameselle-Teijeiro, J., Romero, M.: Artefacts in oral incisional biopsies in general dental practice: a pathology audit. *Oral diseases* **10**(2), 113–117 (2004)
18. Snell, J., Swersky, K., Zemel, R.: Prototypical networks for few-shot learning. *Advances in neural information processing systems* **30** (2017)
19. Taqi, S.A., Sami, S.A., Sami, L.B., Zaki, S.A.: A review of artifacts in histopathology. *Journal of oral and maxillofacial pathology* **22**(2), 279 (2018)
20. The Cancer Genome Atlas Research Network: The cancer genome atlas program. <https://www.cancer.gov/tcga>, accessed: 2025-XX-XX
21. Xu, M., Gupta, S., Hu, X., Li, C., Abousamra, S., Samaras, D., Prasanna, P., Chen, C.: Topocellgen: Generating histopathology cell topology with a diffusion model. In: *Proceedings of the Computer Vision and Pattern Recognition Conference*. pp. 20979–20989 (2025)
22. Xu, X., Kapse, S., Gupta, R., Prasanna, P.: Vit-dae: Transformer-driven diffusion autoencoder for histopathology image analysis. In: *International Conference on Medical Image Computing and Computer-Assisted Intervention*. pp. 66–76. Springer (2023)
23. Xu, X., Kapse, S., Prasanna, P.: Superdiff: A diffusion super-resolution method for digital pathology with comprehensive quality assessment. *Medical Image Analysis* p. 103808 (2025)
24. Xu, Y., He, Z., Shan, S., Chen, X.: Ctrlora: An extensible and efficient framework for controllable image generation. *arXiv preprint arXiv:2410.09400* (2024)
25. Yellapragada, S., Graikos, A., Triaridis, K., Prasanna, P., Gupta, R., Saltz, J., Samaras, D.: Zoomldm: Latent diffusion model for multi-scale image generation. In: *Proceedings of the Computer Vision and Pattern Recognition Conference*. pp. 23453–23463 (2025)
26. Zhang, L., Rao, A., Agrawala, M.: Adding conditional control to text-to-image diffusion models. In: *Proceedings of the IEEE/CVF International Conference on Computer Vision*. pp. 3836–3847 (2023)
27. Zhang, R., Isola, P., Efros, A.A., Shechtman, E., Wang, O.: The unreasonable effectiveness of deep features as a perceptual metric. In: *Proceedings of the IEEE Conference on Computer Vision and Pattern Recognition* (2018)